Journal of Power Sources 244 (2013) 143–148

Contents lists available at SciVerse ScienceDirect

Journal of Power Sources

journal homepage: www.elsevier.com/locate/jpowsour

Modeling the temperature dependence of the discharge behavior of a lithium-ion battery in low environmental temperature

Jaeshin Yi [a], Ui Seong Kim [a], Chee Burm Shin [a,*], Taeyoung Han [b], Seongyong Park [c]

[a] Dept. of Chemical Engineering and Division of Energy Systems Research, Ajou University, Suwon 443-749, Republic of Korea
[b] Vehicle Development Research Lab., GM R&D Center, MI 48090-9055, USA
[c] GM Korea, Inchon 403-714, Republic of Korea

HIGHLIGHTS

- The temperature dependence of the discharge behavior of an LIB in low environmental temperature is modeled.
- The discharge curves of an LIB from modeling agree well with the experimental measurements in low environmental temperature.
- The thermal behaviors from the experiment and modeling are in good agreement with each other in low environmental temperature.

ARTICLE INFO

Article history:
Received 25 October 2012
Received in revised form
22 February 2013
Accepted 25 February 2013
Available online 14 March 2013

Keywords:
Lithium-ion battery
Model
Temperature dependence
Discharge behavior
Low environmental temperature

ABSTRACT

This paper reports a modeling methodology on the temperature dependence of the discharge behavior of a lithium-ion battery (LIB) in low environmental temperature. The discharge curves from the modeling for the discharge rates ranging from 0.5 C to 5 C under the low environmental temperatures of −20, −10 and 0 °C are compared with the experimental data in order to validate the two-dimensional modeling of the potential and current density distributions on the electrodes of an LIB cell as a function of the discharge time during constant-current discharge. The heat generation rates as a result of electrochemical reactions and ohmic heating are calculated to predict the temperature variations of the LIB as a function of the discharge time. The temperature variations obtained from the modeling agree well with the experimental measurements.

1. Introduction

The lithium-ion battery (LIB) is popular in consumer electronics. Beyond consumer electronics, the LIB is also growing in popularity for the automotive applications such as hybrid electric vehicles (HEVs) and battery electric vehicles (BEVs) due to its high energy density, high voltage and low self-discharge rate. Bandhauer et al. [1] stated in their critical review of thermal issues in LIBs that the main barriers to the deployment of large fleets of vehicles on public roads equipped with LIBs continue to be safety, cost (related to cycle and calendar life), and low temperature performance – all challenges that are coupled to thermal effects in the battery.

While the LIBs at room temperature may have the performance including the cell voltage, discharge capacity and power capability adequate for the HEV and BEV applications, their performance is poor at the low environmental temperature that the HEVs and BEVs will experience in normal use. The concern about the plating of lithium metal at the negative electrode also exists during the pulse charge (regen) with high current [2]. There have been many attempts to improve the low-temperature performance of LIBs by developing the electrolytes with higher ionic conductivities at low temperature [3–5]. Many works have been carried out to develop new electrolyte formulations to improve energy utilization in the aerospace industry [6–8]. Jansen et al. used an in situ Li_ySn micro reference electrode to determine the reason for the poor low-temperature performance of LIB [2]. They found that the impedance rise at low temperature is not significantly impacted by the choice of active material, but the electrolyte-interface effect. Abraham et al. studied the low-temperature performance of binder- and carbon-free layered oxide and spinel-oxide electrodes in the coin cells containing a lithium-preloaded $Li_{4/3}Ti_{5/3}O_4$ composite counter electrode [9]. They concluded that low-temperature

* Corresponding author. Tel.: +82 31 219 2388; fax: +82 31 219 1612.
E-mail address: cbshin@ajou.ac.kr (C.B. Shin).

0378-7753/$ – see front matter © 2013 Elsevier B.V. All rights reserved.
http://dx.doi.org/10.1016/j.jpowsour.2013.02.085

performance may be improved by decreasing particle size or changing particle morphology to increase the electrochemically active surface area and by modifying electrolyte-interface to reduce the high activation energy of limiting process. Cho et al. investigated the critical factors affecting the low-temperature performance of LIB from the combination of the three-electrode impedance measurements and the equivalent circuit simulation [10]. They found that the interfacial charge-transfer resistances of the anode and the cathode are two major sources of the low-temperature polarization during the pulse discharge process. Qiao et al. studied electrochemical properties of $Li_3V_2(PO_4)_3$/C were studied from −20 to 65 °C [11]. They reported that the capacity fade at low temperatures is mainly attributed to the reduced conductivity of the electrolyte, the increased impendence of solid electrolyte interface (SEI) and charge-transfer resistance on the electrolyte–electrode interfaces. Even though many researches to improve the low-temperature performance of LIB from different perspectives are still going on, a reliable modeling and simulation tool other than the equivalent circuit models [10,12,13] has not been reported yet to predict the discharge behaviors as well as the thermal behaviors such as the heat generation rate and temperature distributions on the electrodes of a large-size LIB cell for the HEV and BEV applications at low temperature.

Kim et al. recently works presented a method of modeling the temperature dependence of the discharge behavior of an LIB at the environmental temperatures of 15, 25, 35, and 45 °C along with a successful validation of the modeling through the comparison of the modeling results with the experimental measurements [14]. In this work, an extension of the approach of the previous work [14] to the low temperature range from 0 to −20 °C is presented. Modeling results for the variations of voltage and temperature of the LIB cell as a function of time during constant-current discharge are to be compared with the experimental measurements for discharge rates ranging from 0.5 to 5 C and environmental temperatures of −20, −10, and 0 °C to validate the modeling approach presented in this work.

2. Mathematical model

A 14.6 Ah LIB comprising $LiMn_2O_4$ positive electrodes, graphite negative electrodes, and porous separators impregnated with plasticized electrolyte from LG Chem. was modeled in this work. A cell consisting of two parallel plate electrodes of the battery shown in Fig. 1 was chosen because an LIB consists of the same repeating units of positive and negative electrode plates, polymer electrolytes and separators. In Fig. 1, the current collecting tabs are the current collectors extending outside the rectangular electrodes and they do not contain the electrode (active) material. Fig. 1 shows a schematic diagram of the current flow in the cell during discharge. The distance between the electrodes was assumed to be so small that the current flow between the electrodes is perpendicular to the electrodes. The modeling procedure used to calculate the potential and current density distribution on the electrodes was similar to that used by Kwon et al. [15]. From the continuity of the current on the electrodes during discharge, the following Poisson equations for the potentials in the positive and negative electrodes can be derived

$$\nabla^2 V_p = -r_p J \quad \text{in } \Omega_p \tag{1}$$

$$\nabla^2 V_n = +r_n J \quad \text{in } \Omega_n \tag{2}$$

where V_p and V_n are the potentials (V) of the positive and negative electrodes, respectively, r_p and r_n are the resistances (Ω) of the positive and negative electrodes, respectively, and J is the current density (current per unit area (A m^{-2})) transferred through the

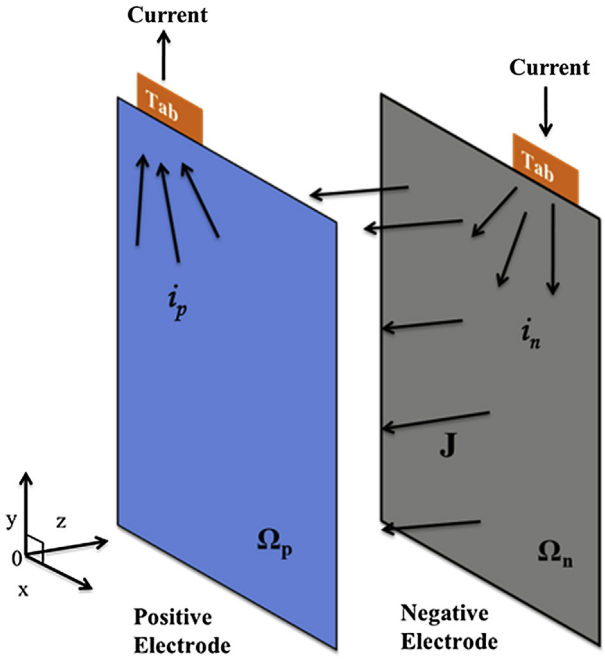

Fig. 1. Schematic diagram of the current flow in the parallel plate electrodes of a battery.

separator from the negative electrode to the positive electrode. Ω_p and Ω_n denote the domains of the positive and negative electrodes, respectively. The resistances, r_p and r_n, are calculated as described in Refs. [15–17]. The relevant boundary conditions for V_p and V_n are given in Ref. [15].

The current density, J, of Eqs. (1) and (2) is a function of the potential difference between the positive and negative electrodes, $(V_p - V_n)$. The functional form depends on the polarization characteristics of the electrodes. In this work, the following polarization expression used by Tiedemann and Newman [18] and Newman and Tiedemann [19] was adopted

$$J = Y(V_p - V_n - U) \tag{3}$$

where Y and U are the fitting parameters. As suggested by Gu [20], U and Y were expressed as functions of the depth of discharge (DOD) as follows:

$$U = a_0 + a_1(\text{DOD}) + a_2(\text{DOD})^2 + a_3(\text{DOD})^3 \tag{4}$$

$$Y = a_4 + a_5(\text{DOD}) + a_6(\text{DOD})^2 + a_7(\text{DOD})^3 + a_8(\text{DOD})^4 + a_9(\text{DOD})^5 \tag{5}$$

where $a_0 \sim a_9$ are the constants that provide the best fit of the modeling results to the experimental data at an environmental temperature of 0 °C. The usual approach of linear or nonlinear parameter estimation cannot be used in this work, because the explicit functional relationship between the cell voltage and the values of $a_0 \sim a_9$ is not identifiable. The approach adopted in this work is the "art" of trial and error, which may require exhaustive enumeration. One way to alleviate the efforts of trial and error is to use the low order polynomials of DOD in Eqs. (4) and (5) to obtain a rough fit of the experimental data and then to increase gradually the orders of polynomials to get a more refined fit. The values of $a_0 \sim a_9$ used to calculate the potential and current density distribution on the electrodes at an environmental temperature of 0 °C are listed in Table 1. In order to model the discharge behaviors at

Table 1
Fitting parameters used to calculate the potential and current density distributions on the electrodes at an environmental temperature of 0 °C.

Parameter	Value
a_0 (V)	4.07
a_1 (V)	−1.23
a_2 (V)	2.385
a_3 (V)	−2.213
a_4 (Am^{-2})	44.7688
a_5 (Am^{-2})	−245.4732
a_6 (Am^{-2})	1492.0478
a_7 (Am^{-2})	−3790.085
a_8 (Am^{-2})	4194.6171
a_9 (Am^{-2})	−1701.285

Table 2
Parameters used for the thermal modeling.

Component	Density (kg m^{-3})	Heat capacity (J kg^{-1} °C^{-1})	Thermal conductivity (W m^{-1} °C^{-1})	Ref.
Current collector of positive electrode	2.7×10^3	0.9×10^3	204	[23]
Electrode material of positive electrode	1.5×10^3	0.7×10^3	5	[14]
Current collector of negative electrode	8.96×10^3	0.39×10^3	386	[23]
Electrode material of negative electrode	2.5×10^3	0.7×10^3	5	[14]
Separator	1.2×10^3	0.7×10^3	1	[14]
Pouch	1.15×10^3	1.9×10^3	0.16	[14]

the different environmental temperatures other than 0 °C in low environmental temperature, Y and U should be modified as follows:

$$Y = Y_0 \exp\left\{C_1\left(\frac{1}{T_{abs}} - \frac{1}{T_{abs,0}}\right)\right\} \quad (6)$$

$$U = U_0 - C_2(T_{abs} - T_{abs,0}) \quad (7)$$

where Y_0 and U_0 are the values of Y and U at an environmental temperature of 0 °C, T_{abs} and $T_{abs,0}$ are the absolute temperature (K) of the environmental temperature other than 0 °C and that of 0 °C, respectively, and C_1 and C_2 are constants to be determined to fit the temperature dependence of Y and U. The reason to choose the value of $T_{abs,0}$ as 0 °C will be discussed later in the section of results and discussion. The functional relationship of Y with T_{abs} suggested in Eq. (6) was deduced from the Arrhenius equation which gives the relationship between the reaction rate constant and the absolute temperature as shown below [21]:

$$k = Ae^{-E_a/RT_{abs}} \quad (8)$$

where k is the rate constant of chemical reactions (s^{-1}; for the first order reaction), A is the pre-exponential factor (s^{-1}; for the first order reaction), E_a is the activation energy (J mol^{-1}), and R is the gas constant (J mol^{-1} K^{-1}). The functional relationship of U with T_{abs} suggested in Eq. (7) was deduced from the Nernst equation which gives the relationship between the equilibrium potential of the battery cell and the absolute temperature [21]:

$$E = E^0 - \frac{RT_{abs}}{zF}\ln Q \quad (9)$$

where E is the cell potential (V), E^0 is the standard cell potential (V), z is the number of moles of electrons transferred in the cell reaction, and Q is the reaction quotient. The values of C_1 and C_2 used in this work were 2000 and −0.101, respectively.

By solving the equations listed previously, the distribution of the current density, J, on the electrodes can be obtained as a function of the position on the electrode and time. Therefore, the DOD varies along with the position on the electrode and time elapsed during discharge. The distribution of DOD on the electrode can be calculated from the distribution of J as follows:

$$DOD = \frac{\int_0^t J\,dt}{Q_T} \quad (10)$$

where t is the discharge time (s) and Q_T is the capacity per unit area (Ah m^{-2}) of the electrodes. Because the discharge capacity of a battery cell in low environmental temperature is a strong function of temperature, the capacity used to calculate DOD in Eq. (10) is measured experimentally with the discharge rate of 1 C at a given temperature.

The thermal modeling procedure employed to calculate the temperature distribution on the electrodes is similar to that used by Kim et al. [16,17]. Because the heat flux in z direction of Fig. 1 is negligible as compared to those in x and y directions of Fig. 1 based on the calculation results from the three dimensional thermal modeling of Yi et al. [22] on the same LIB cell modeled in the present work, the transient two-dimensional equation of heat conduction can be written as follows:

$$\rho C_p \frac{\partial T}{\partial t} = \frac{\partial}{\partial x}\left(k_x \frac{\partial T}{\partial x}\right) + \frac{\partial}{\partial y}\left(k_y \frac{\partial T}{\partial y}\right) + q - q_{conv} \quad (11)$$

where ρ is the density (kg m^{-3}), C_p is the volume averaged specific heat capacity at constant pressure (J kg^{-1} °C^1), T is the temperature

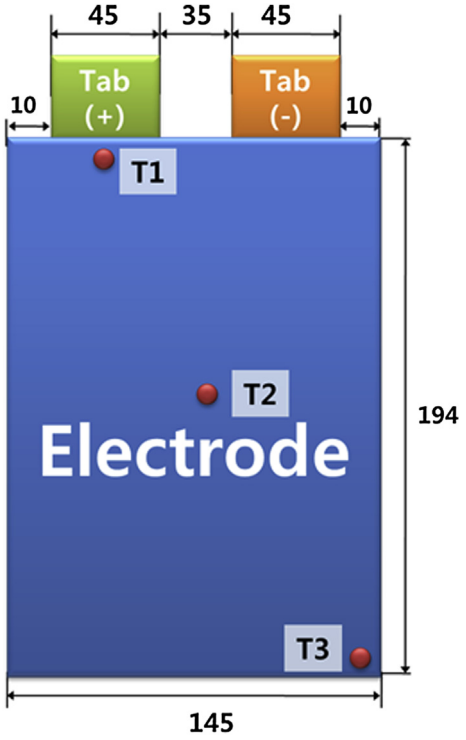

Fig. 2. The dimensions of the electrodes and the positions of the tabs of a 14.6 Ah LIB from LG Chem and the three positions T1, T2 and T3 where J-type thermocouples are placed to measure the temperature variations at three positions on the surface of battery cell. Dimensions are in mm.

(°C), k_x and k_y are the effective thermal conductivities along the x and y directions (refer Fig. 1 for the x and y directions) (W m^{-1} °C^{-1}), respectively, q is the heat generation rate per unit volume (W m^{-3}), and q_{conv} is the heat dissipation rate (W m^{-3}) through the surfaces of the battery by convection. The effective thermal conductivities of the various compartments of the cell can be estimated based on the equivalent networks of the parallel and series thermal resistances of the cell components [16,17].

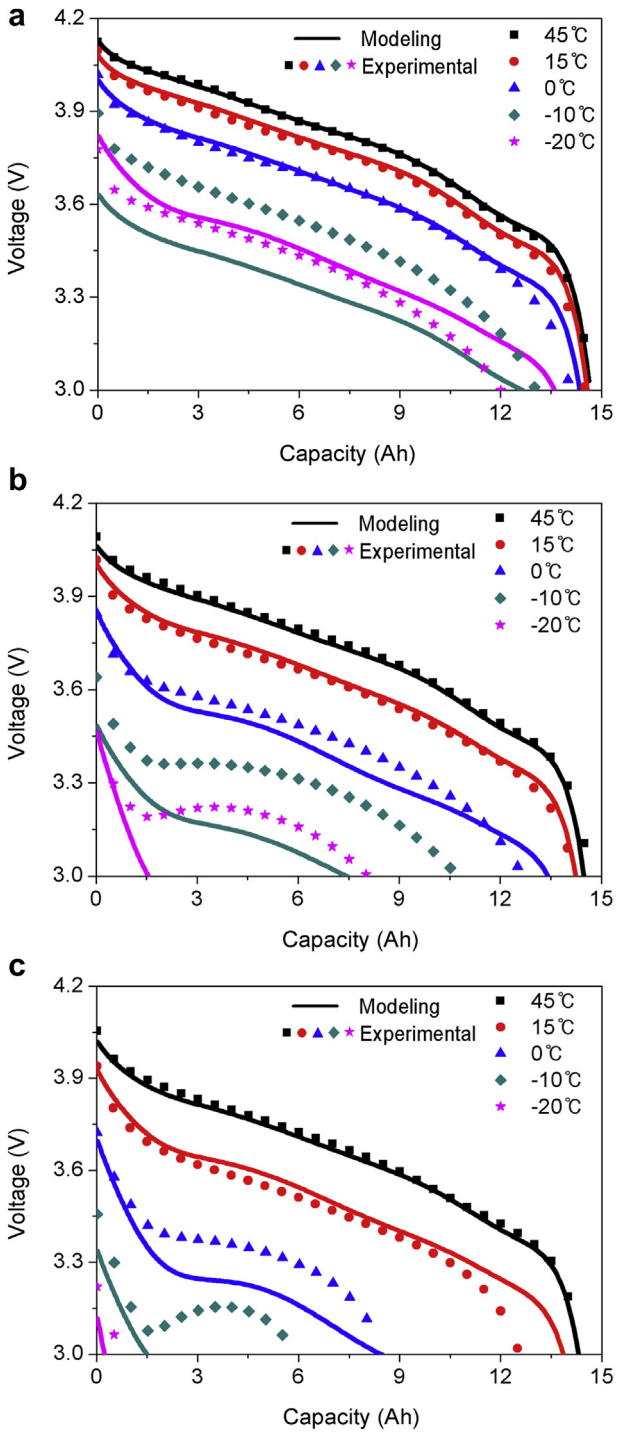

Fig. 3. Comparisons between the discharge curves calculated from the modeling by using the same parameters of $a_0 \sim a_9$ obtained at 25 °C and the experimental data for discharge rates ranging of (a) 1 C, (b) 3 C and (c) 5 C, respectively, at the environmental temperatures of −20, −10, 0, 15, and 45 °C.

The heat generation rate, q, is given as follows:

$$q = aJ\left[V_{oc} - V_{cell} - T\frac{dV_{oc}}{dT}\right] + a_p\frac{|\nabla V_p|^2}{r_p} + a_n\frac{|\nabla V_n|^2}{r_n} \quad (12)$$

where a is the specific area of the battery (m^{-1}), J is the current density (A m^{-2}) calculated by Eq. (7), V_{oc} is the open-circuit potential of the cell (V), V_{cell} is the cell voltage (V) obtained through the solutions of Eqs. (1) and (2), a_p and a_n are the specific area of the positive and negative electrodes (m^{-1}), respectively, and $|\nabla V_p|$ and $|\nabla V_n|$ are the magnitudes of the gradient vectors of ∇V_p and ∇V_n obtained by Eqs. (1) and (2) (A m^{-1}), respectively. The detailed definition of each term on the right-hand side of Eq. (12) is described in Refs. [16,17]. The heat dissipation rate, q_{conv}, is derived as follows

$$q_{conv} = \frac{2h}{d}(T - T_{air}) \quad (13)$$

where h is the convective heat transfer coefficient on the surfaces of the battery (W m^{-2} °C^{-1}), d is the thickness of the battery in the direction perpendicular to the parallel electrodes (m), and T_{air} is the ambient temperature (°C). This term is rendered by approximating a three-dimensional object into a two-dimensional one, as shown in Eq. (11). The values of h and d used in this work were 8 W m^{-2} °C^{-1} and 0.0057 m, respectively. The convective boundary condition applied to the boundaries of the electrode is the one reported by Kim et al. [16]. Table 2 lists and the parameters used for the thermal modeling.

3. Results and discussion

The solutions to the governing Eqs. (1), (2) and (11) subject to the associated boundary conditions were obtained using the finite element method. In order to test the validity of the model, discharge experiments were carried out at room temperature of 25 °C using a 14.6 Ah battery fabricated by LG Chem., of which the dimensions of the electrodes and the positions of the tabs are shown in Fig. 2. As shown in Fig. 2, J-type thermocouples were placed to measure the temperature variations at three positions of T1, T2 and T3 on the surface of battery cell where the maximum, intermediate and minimum temperatures, respectively, are expected to be detected during discharge. To show that the modeling approach of Kim et al. [14] fails to the discharge behavior of the LIB cell in the environmental temperature lower than 0 °C, the

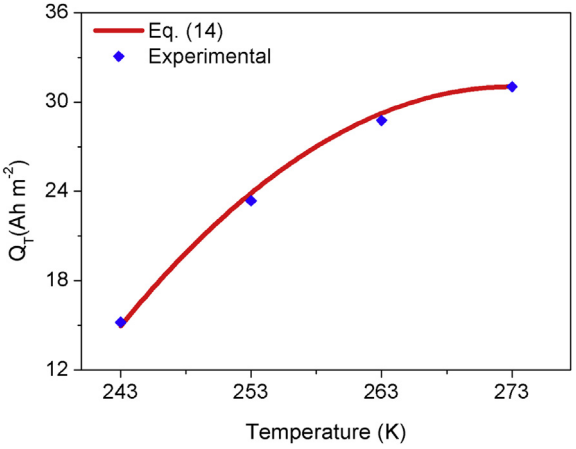

Fig. 4. Comparison between Q_T calculated by Eq. (14) and the experimental data in the range of environmental temperature from −30 to 0 °C.

discharge curves were calculated by using the same parameters of $a_0 \sim a_9$ obtained at 25 °C. Fig. 3(a), (b) and (c) show the comparisons between the discharge curves calculated from the modeling by using the same parameters of $a_0 \sim a_9$ obtained at 25 °C and the experimental data for discharge rates ranging of 1 C, 3 C and 5 C, respectively, at the environmental temperatures of −20, −10, 0, 15, and 45 °C. The experimental discharge curves agree well with those obtained from the modeling at environmental temperatures of 15 °C and 45 °C as validated in Kim et al. [14]. The discrepancy between the modeling results and the experimental data increases as the environmental temperature decreases farther from 0 °C and the discharge rate increases. Below the temperature of −10 °C and at the discharge rate higher than 3 C, the modeling approach of Kim et al. [14] totally loses the capability to predict the discharge behavior of the LIB cell.

In order to establish the capability to predict the discharge behavior of the LIB cell even in the low temperature and high discharge rate, many trials and errors were made. One of the

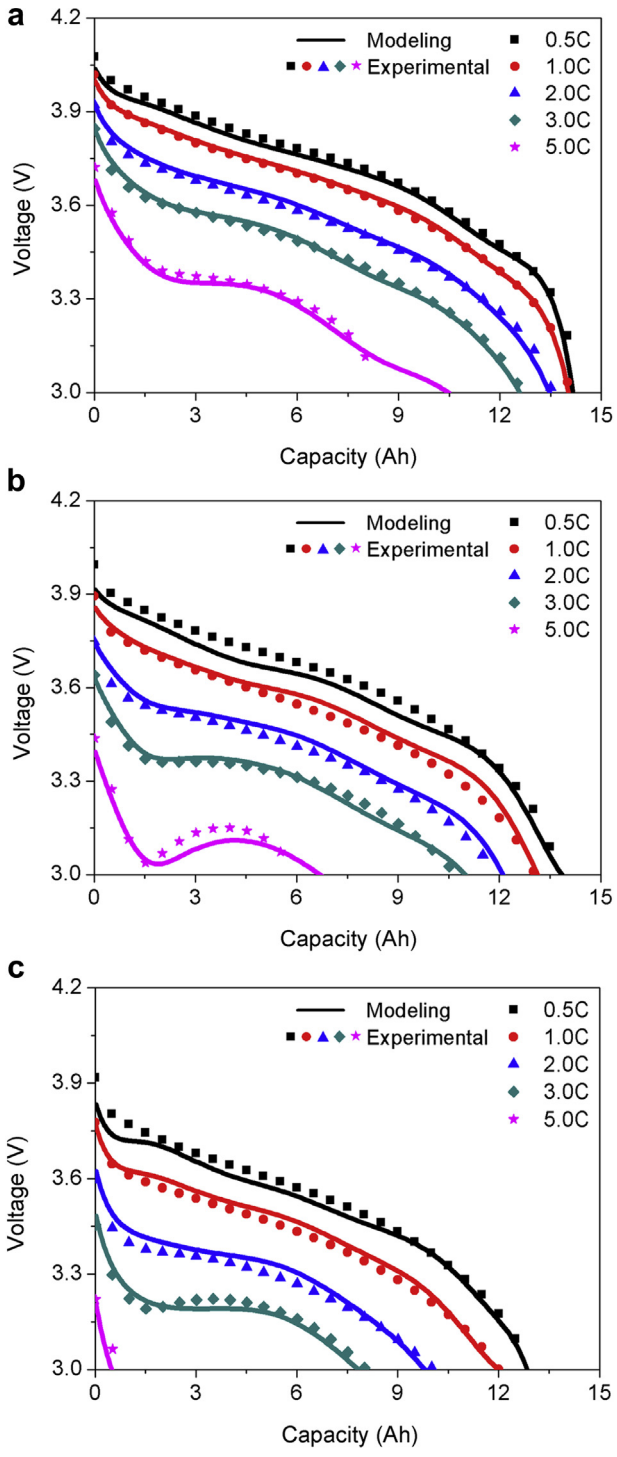

Fig. 5. Comparisons between the calculated discharge curves obtained from the modeling approach suggested in this work instead of that in Kim et al. [14] and the experimental data for discharge rates ranging from 0.5 C to 5 C at the environmental temperatures of (a) 0 °C, (b) −10 °C and (c) −20 °C, respectively.

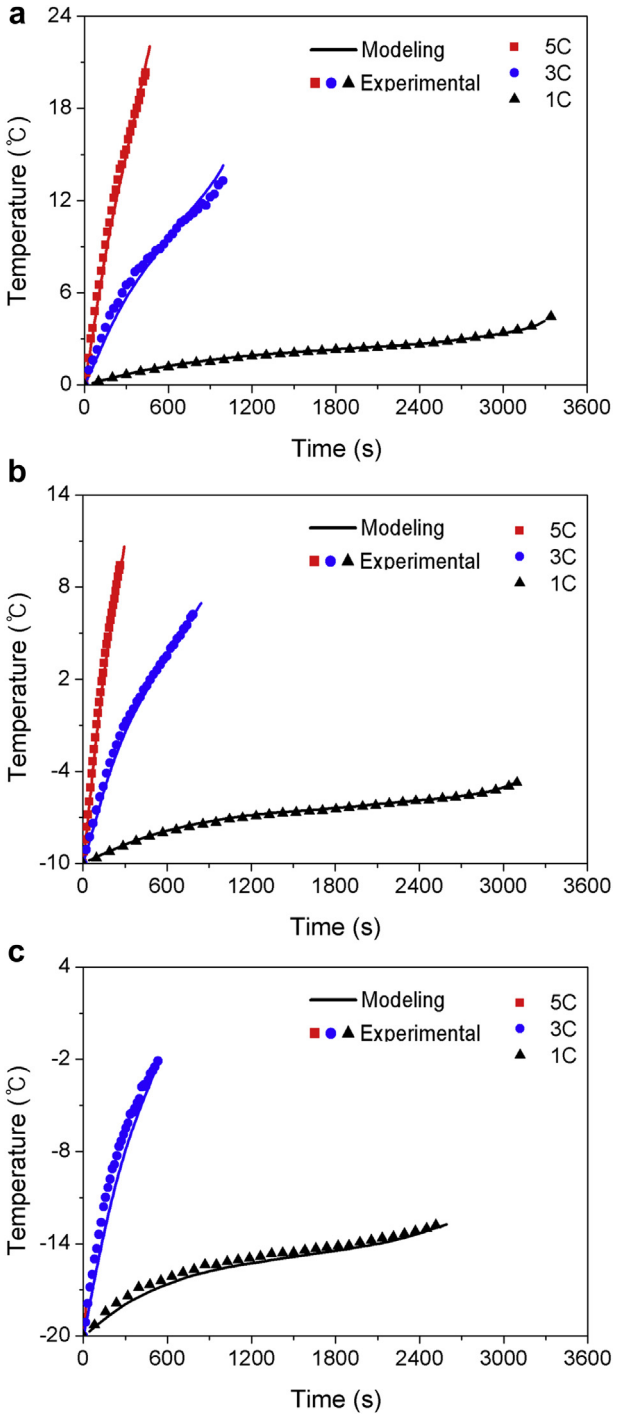

Fig. 6. Comparison between the temperatures at T1 of Fig. 2 under the environmental temperatures of (a) 0 °C, (b) −10 °C and (c) −20 °C, respectively, obtained from the experimental measurements and those predicted by the model.

successful approaches to be presented in this work is to use the same strategy of Kim et al. [14] using Eqs. (6) and (7) with taking 0 °C as the value of $T_{abs,0}$ in the low-temperature region below 0 °C instead of 25 °C as in Kim et al. [14]. In addition to taking a different value for $T_{abs,0}$, another measure should be taken for the capacity per unit area (Ah m^{-2}) of the electrodes in Eq. (10). As one can conjecture from the discharge curves shown in Fig. 3, the discharge capacity drops significantly as the temperature decreases below 0 °C. In order to express a strong functional relationship in low environmental temperature between the discharge capacity of an LIB cell and the temperature, the capacity is measured experimentally in low environmental temperature through the discharge of the battery cell with a discharge rate of 1 C at a given temperature. Q_T used to calculate DOD in Eq. (14) can be obtained by dividing the experimentally measured discharge capacity with 1 C discharge rate by the electrode area. In this work, an additional functional relationship between Q_T and T_{abs} is introduced as

$$Q_T = Q_{T,0} - C_3 \left(T_{abs} - T_{abs,0}\right)^2 \quad (14)$$

where $Q_{T,0}$ is Q_T at $T_{abs,0}$. Eq. (14) contains only one fitting parameter, C_3, but it still provides a good fit of the experimentally measured data of Q_T shown in Fig. 4. The value of C_3 used in this work was 0.01789. Fig. 5(a), (b) and (c) show the comparisons between the calculated discharge curves obtained from the modeling approach suggested in this work instead of that in Kim et al. [14] and the experimental data for discharge rates ranging from 0.5 C to 5 C at the environmental temperatures of 0 °C, −10 °C and −20 °C, respectively. The experimental discharge curves agree well with those obtained from the modeling. This means that the modeling methodology in this work used for the potential and current density distributions on the electrodes can be safely applied to the environmental temperature below 0 °C.

Fig. 6(a), (b) and (c) show the comparison between the temperatures at T1 of Fig. 2 under the environmental temperatures of 0 °C, −10 °C and −20 °C, respectively, obtained from the experimental measurements and those predicted by the model. The temperatures at T1 obtained from the experiment and modeling are in good agreement with each other over the whole range of DODs at the various discharge rates. We also confirmed the good agreement between the temperature variations with time at T2 and T3 during discharge observed from the experiment and those from the modeling, but we did not include these results since they appeared to be redundant.

4. Conclusions

A mathematical procedure is developed to study the temperature dependence of the discharge behaviors of an LIB in low environmental temperature. To accommodate the temperature dependence of the discharge behavior of a LIB in low environmental temperature, the key modeling parameters obtained at the environmental temperature of 0 °C are modified based on the well-known principles of the Arrhenius equation of chemical kinetics and the Nernst equation of electrochemical thermodynamics. In order to express a strong functional relationship in low environmental temperature between the discharge capacity of an LIB cell and the temperature, the capacity is measured experimentally in low environmental temperature through the discharge of the battery cell with a discharge rate of 1 C at a given temperature. The functional relationship between the discharge capacity and the temperature is expressed as a quadratic function. Modeling results for the variations of voltage and temperature of the LIB cell as a function of time during constant-current discharge are compared with the experimental measurements for discharge rates ranging from 0.5 to 5 C and environmental temperatures of −20, −10, and 0 °C to validate the modeling approach presented in this work. The modeling results for the variations of voltage and temperature as a function of discharge time are in good agreement with the experimental data. The modeling methodology presented in this study may contribute to the accurate prediction of the performance of LIB as a function of the environmental temperature below 0 °C.

Acknowledgments

This study was supported by General Motors Corporation. One of the authors (C. B. Shin) acknowledges the partial financial support provided by the National Research Foundation of Korea (NRF 2009-0064626 and NRF 2010–0025353) and the Ministry of Commerce, Industry and Energy of Republic of Korea (2007-E-1D25-P-02-0-00) for this work.

References

[1] T.M. Bandhauer, S. Garimella, T.F. Fuller, J. Electrochem. Soc. 158 (2011) R1–R25.
[2] A.N. Jansen, D.W. Dees, D.P. Abraham, K. Amine, G.L. Henriksen, J. Power Sources 174 (2007) 373–379.
[3] M.S. Ding, K. Xu, S.S. Zhang, K. Amine, G.L. Henriksen, T.R. Jow, J. Electrochem. Soc. 148 (2001) A1196–A1204.
[4] M.S. Ding, T.R. Jow, J. Electrochem. Soc. 150 (2003) A620–A628.
[5] M.S. Ding, T.R. Jow, J. Electrochem. Soc. 151 (2004) A2007–A2015.
[6] M.C. Smart, B.V. Ratnakumar, S. Surampudi, J. Electrochem. Soc. 146 (1999) 486–492.
[7] B.V. Ratnakumar, M.C. Smart, S. Surampudi, J. Power Sources 97-98 (2001) 137–139.
[8] M.C. Smart, B.V. Ratnakumar, L.D. Whitcanack, K.B. Chin, S. Surampudi, H. Croft, D. Tice, R. Staniewicz, J. Power Sources 119-121 (2003) 349–358.
[9] D.P. Abraham, J.R. Heaton, S.-H. Kang, D.W. Dees, A.N. Jansen, J. Electrochem. Soc. 155 (2008) A41–A47.
[10] H.-M. Cho, W.-S. Choi, J.-Y. Go, S.-E. Bae, H.-C. Shin, J. Power Sources 198 (2012) 273–280.
[11] Y.Q. Qiao, J.P. Tu, X.L. Wang, C.D. Gu, J. Power Sources 199 (2012) 287–292.
[12] M.W. Verbrugge, R.Y. Ying, J. Electrochem. Soc. 154 (2007) A949–A956.
[13] D. Dees, E. Gunen, D. Abraham, A. Jansen, J. Prakash, J. Electrochem. Soc. 155 (2008) A603–A613.
[14] U.S. Kim, J. Yi, C.B. Shin, T. Han, S. Park, J. Electrochem. Soc. 158 (2011) A611–A618.
[15] K.H. Kwon, C.B. Shin, T.H. Kang, C.-S. Kim, J. Power Sources 163 (2006) 151–157.
[16] U.S. Kim, C.B. Shin, C.-S. Kim, J. Power Sources 180 (2008) 909–916.
[17] U.S. Kim, C.B. Shin, C.-S. Kim, J. Power Sources 189 (2009) 841–846.
[18] W. Tiedemann, J. Newman. PV 79-1, in: S. Gross (Ed.), Battery Design and Optimization, The Electrochemical Society Proceeding Series, Pennington, NJ, 1979, p. 39.
[19] J. Newman, W. Tiedemann, J. Electrochem. Soc. 140 (1993) 1961–1968.
[20] H. Gu, J. Electrochem. Soc. 130 (1983) 1459–1464.
[21] A.J. Bard, L.R. Falkner, Electrochemical Methods: Fundamentals and Applications, second ed., John Wiley and Sons, Inc., New York, 2001.
[22] J. Yi, U.S. Kim, C.B. Shin, T. Han, S. Park, J. Electrochem. Soc. 160 (2013) A437–A443.
[23] S.C. Chen, C.C. Wan, Y.Y. Wang, J. Power Sources 140 (2005) 111–124.